Available online at www.sciencedirect.com
ScienceDirect
Journal of Sound and Vibration 304 (2007) 932–947
JOURNAL OF SOUND AND VIBRATION
www.elsevier.com/locate/jsvi

A comparison of infinite Timoshenko and Euler–Bernoulli beam models on Winkler foundation in the frequency- and time-domain

P. Ruge, C. Birk*

Lehrstuhl Dynamik der Tragwerke, Fakultät Bauingenieurwesen, Technische Universität Dresden, D-01062 Dresden, Germany

Received 3 August 2006; received in revised form 19 March 2007; accepted 2 April 2007

Abstract

This paper deals with the dynamic analysis of infinite beam models. The translational and the rotational dynamic stiffness of both Timoshenko and Euler–Bernoulli beams on Winkler foundation are derived and compared in the frequency-domain. The situation of vanishing elastic foundation is included as a special case. Here, special emphasis is placed on the asymptotic behaviour of the derived stiffness expressions for high frequencies, since this is of importance in case of transient excitations. It is shown that the dynamic stiffness of the infinite Timoshenko beam follows a linear function of $i\omega$, whereas rational powers of $i\omega$ are involved in case of Euler–Bernoulli's model. The stiffness formulations can be transformed into the time-domain using the mixed-variables technique. This is based on a rational approximation of the low-frequency force–displacement relationship and a subsequent algebraic splitting process. At the same time, the high-frequency asymptotic dynamic stiffness is transformed into the time-domain in closed-form. It is shown that the Timoshenko beam is equivalent to a simple dashpot in the high-frequency limit, whereas Euler–Bernoulli's beam model leads to fractional derivatives of the unknown state variables in an equivalent time-domain description. This finding confirms the superiority of Timoshenko's model especially for high frequencies and transient excitations. Numerical examples illustrate the differences with respect to the two beam models and demonstrate the applicability of the proposed method for the time-domain transformation of force–displacement relationships.

1. Introduction

This paper is devoted to the dynamic analysis of infinite beams in the frequency- and time-domain, with special emphasis on the asymptotic behaviour for high frequencies.

Continuous beam models are of practical importance in railway engineering. Within this context, a comprehensive review of historical literature and recently published methods to model vehicle and track in dynamic interaction problems has been given in Ref. [1]. There, the theoretical importance of classical continuous models is substantiated by fifteen references and the adequacy of simple railway models to certain types of problems is addressed.

*Corresponding author. Tel.: +49 351 4633 5325; fax: +49 351 4633 4096.
E-mail addresses: Peter.Ruge@tu-dresden.de (P. Ruge), Carolin.Birk@tu-dresden.de (C. Birk).

0022-460X/$ - see front matter © 2007 Elsevier Ltd. All rights reserved.
doi:10.1016/j.jsv.2007.04.001

In connection with railway engineering applications both beam models based on Euler–Bernoulli's [2–4] and on Timoshenko's beam theory [5–9] have been used. It is a well-known fact, that shear deformation and rotatory inertia should be taken into account when considering the dynamic response of beams [10,11]. This is particularly important if mode shapes and eigenfrequencies of finite beams are computed [12–14]. Euler–Bernoulli's theory is sufficiently accurate only for wave lengths approximately $\lambda \geqslant 10r$ or frequencies $f < c/10r$ with the velocity c of travelling waves in case of beams with circular cross-section of radius r as can be seen from a figure in Ref. [15, p. 325]. Consequently, especially for higher frequencies [16], dynamic analyses of beams under arbitrary transient excitations should be based on Timoshenko's theory.

Another important aspect of the use of the above beam models in the context of railway engineering is the infinite extent of the system. For transient excitations, a correct representation of radiation damping is necessary. Sun [3,17] and Kargarnovin [7,8] derived closed-form analytical solutions for infinite Euler–Bernoulli and Timoshenko beams on different types of foundation under harmonic loads using complex Fourier transformation together with the residue and convolution integral theorem. In this paper, dynamic stiffness coefficients relating the amplitude of a time-harmonic unit force or moment to that of the resulting displacement or rotation, respectively, are derived for both the Timoshenko and Euler–Bernoulli beam on elastic Winkler foundation. The former is an extension of the derivation presented in Ref. [16], the latter is a summary of material published previously in Refs. [18,19]. Here, special emphasis is placed on the high-frequency asymptotic behaviour of the dynamic stiffness. The resulting limit values for the dynamic stiffness confirm the discrepancy between Timoshenko's and Euler–Bernoulli's model in the medium to high frequency range. This is of special importance for transient time-domain calculations. In this paper, time-domain models of the two different infinite beams are obtained using the mixed-variables technique [20]. The latter is based on a rational approximation of a given set of frequency-stiffness pairs and a subsequent algebraic splitting process. Here, the asymptotic value of the dynamic stiffness for high frequencies is transformed into the time-domain in closed-form. This leads to first-order time-derivatives of the unknown state variables in case of the Timoshenko beam. However, fractional derivatives are obtained in case of Euler–Bernoulli's model. In both cases, the resulting time-domain formulations can be used as absorbing boundaries in transient analyses of finite, inhomogeneous and possibly nonlinear railway–vehicle analyses.

2. Dynamic stiffness of infinite beams

In this paper, the dynamic behaviour of infinite beams resting on a Winkler foundation is described in the frequency-domain in order to formulate the dynamic stiffness relationship,

$$\begin{bmatrix} \hat{F} \\ \hat{M} \end{bmatrix} = \mathbf{K}(\mathrm{i}\omega) \begin{bmatrix} \hat{w} \\ \hat{\varphi} \end{bmatrix}, \quad \hat{\mathbf{f}} = \mathbf{K}\hat{\mathbf{d}}, \quad \mathbf{f}(t) = \hat{\mathbf{f}}\mathrm{e}^{\mathrm{i}\omega t}, \quad \mathbf{d}(t) = \hat{\mathbf{d}}\mathrm{e}^{\mathrm{i}\omega t}, \tag{1}$$

between the deformations $\hat{\mathbf{d}}$ and the generalized forces $\hat{\mathbf{f}}$ in the point where $\mathbf{f}(t)$ acts onto the beam. The definition of the above forces and deformations is shown in Fig. 1 for a Timoshenko beam on elastic foundation.

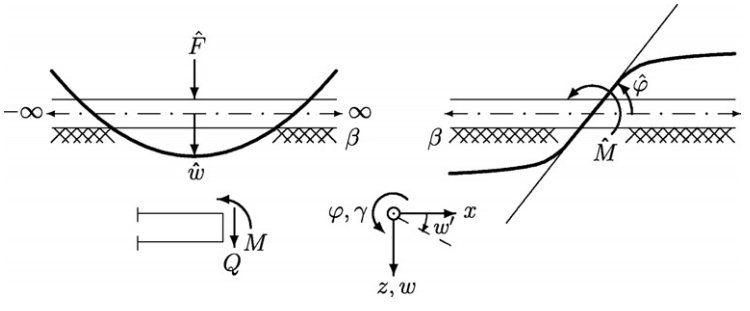

Fig. 1. Infinite Timoshenko beam. Definition of forces and deformations.

2.1. Infinite Timoshenko beam

If shear deformations are considered, the slope of the deflection curve $w(x)$ depends not only on the rotation φ of the beam cross-section but also on the shear angle γ:

$$\frac{\partial}{\partial x} w(x,t) = -\varphi(x,t) - \gamma(x,t). \tag{2}$$

Bending moment $M(x,t)$ and shear force $Q(x,t)$ are related to the corresponding deformations,

$$\begin{aligned} M(x,t) &= EI \frac{\partial}{\partial x} \varphi(x,t), \\ Q(x,t) &= -\kappa GA\gamma = \kappa GA\left[\varphi(x,t) + \frac{\partial}{\partial x} w(x,t)\right], \end{aligned} \tag{3}$$

where $EI\,[\mathrm{Nm}^2]$ is the flexural stiffness, $A\,[\mathrm{m}^2]$ the cross-sectional area, $G\,[\mathrm{N/m}^2]$ the shear modulus from $E = 2G(1+\nu)$ with Poisson's ratio ν, and κ is the shear coefficient. κ depends on the shape of the cross-section, Poisson's ratio and the considered frequency range. For circles, rectangles and thin-walled cross-sections, Cowper [21] gave several relations. For high-frequency modes, values published by Mindlin [22] should be considered. The elasticity equations (3) are coupled with the dynamic equilibrium concerning the forces,

$$\frac{\partial}{\partial x} Q(x,t) + q(x,t) - \beta w(x,t) = \rho A \ddot{w}(x,t) \tag{4}$$

and the moments,

$$\frac{\partial}{\partial x} M(x,t) - Q(x,t) + m(x,t) = \rho I \ddot{\varphi}(x,t), \tag{5}$$

where $\rho\,[\mathrm{kg/m}^3]$ is the mass density per volume, $I\,[\mathrm{m}^4]$ the second moment of area about the y-axis through the centre of the cross-section, $q(x,t)\,[\mathrm{N/m}]$ is the prescribed distributed load on the beam, $m(x,t)\,[\mathrm{Nm/m}]$ the prescribed distributed moment along the beam and $\beta\,[\mathrm{N/m}^2]$ is the distributed stiffness of the Winkler foundation.

The constitutive relations (3) together with the equations of motion (4), (5) define the governing differential equations for the displacements $w(x,t)$ and the rotation $\varphi(x,t)$:

$$\begin{aligned} -\kappa GA\left(\frac{\partial \varphi}{\partial x} + \frac{\partial^2 w}{\partial x^2}\right) + \beta w + \rho A \ddot{w} &= q, \\ \kappa GA\left(\varphi + \frac{\partial w}{\partial x}\right) - EI\,\frac{\partial^2 \varphi}{\partial x^2} + \rho I \ddot{\varphi} &= m. \end{aligned} \tag{6}$$

A wave-type representation

$$\begin{bmatrix} w(x,t) \\ \varphi(x,t) \end{bmatrix} = \begin{bmatrix} \hat{w} \\ \hat{\varphi} \end{bmatrix} \mathrm{e}^{-x\sqrt{\lambda} + \mathrm{i}\omega t}, \tag{7}$$

solves the homogeneous part of Eqs. (6) yielding a quadratic equation for the roots λ:

$$\lambda^2 - \lambda\,\frac{\kappa GAM_R + EIM_{T\beta}}{\kappa GAEI} + \frac{M_{T\beta}(M_R + \kappa GA)}{\kappa GAEI} = 0. \tag{8}$$

The new parameters are related to rotational (R) and translational (T) properties:

$$\begin{aligned} M_{T\beta} &= \rho A(\mathrm{i}\omega)^2 + \beta, \\ M_R &= \rho I(\mathrm{i}\omega)^2, \\ c_T^2 &= \frac{\kappa G}{\rho}, \\ c_R^2 &= \frac{E}{\rho}. \end{aligned} \tag{9}$$

Use of a dimensionless frequency η,

$$\eta^2 = \omega^2 \frac{\rho A}{\beta} = \frac{\kappa G A}{\beta} \frac{\omega^2}{c_T^2}, \tag{10}$$

facilitates the solution of the square root equation (8) for λ:

$$\lambda_1 = \frac{1}{2} \frac{\beta}{\kappa G A} \left[(1-\eta^2) + \frac{c_T^2}{c_R^2} (-\eta^2 + \sqrt{R}) \right], \tag{11}$$

$$\lambda_2 = \frac{1}{2} \frac{\beta}{\kappa G A} \left[(1-\eta^2) + \frac{c_T^2}{c_R^2} (-\eta^2 - \sqrt{R}) \right], \tag{12}$$

$$R = 4 \frac{\kappa G A^2}{I\beta} \frac{c_R^2}{c_T^2} (\eta^2 - 1) + \left[\frac{c_R^2}{c_T^2} (1-\eta^2) + \eta^2 \right]^2. \tag{13}$$

In the special case $\eta^2 = 1$, one of the two eigenvalues $\lambda_{1,2}$ degenerates to zero.

$$\lambda_{1,2} = \frac{1}{2} \frac{\beta}{\kappa G A} \frac{c_T^2}{c_R^2} (-1 \pm 1), \quad \lambda_1 = 0, \quad \lambda_2 = -\frac{\beta}{\kappa G A} \frac{c_T^2}{c_R^2} = -\frac{\beta}{EA}. \tag{14}$$

Moreover, $\lambda_1 = 0$ is obtained if

$$(1-\tilde{\eta}^2) + \frac{c_T^2}{c_R^2} (-\tilde{\eta}^2 + \sqrt{R}) \stackrel{!}{=} 0. \tag{15}$$

This yields

$$4 \frac{\kappa G A^2}{I\beta} (\tilde{\eta}^2 - 1) = 4\tilde{\eta}^2 (\tilde{\eta}^2 - 1). \tag{16}$$

Thus, the infinite Timoshenko beam on a Winkler foundation is characterized by two typical frequencies,

$$\tilde{\eta}_1 = 1, \quad \tilde{\eta}_2^2 = \frac{\kappa G A^2}{I\beta}, \tag{17}$$

$$\tilde{\omega}_1^2 = \frac{\beta}{\rho A}, \quad \tilde{\omega}_2^2 = \frac{\kappa G A}{\rho I} = c_T^2 \frac{A}{I}. \tag{18}$$

In the special case of vanishing Winkler foundation, $\beta = 0$, the roots $\lambda_{1,2}$ simplify as follows:

$$\lambda_1^{\beta=0} = -\frac{\omega^2}{2} \left[\left(\frac{1}{c_T^2} + \frac{1}{c_R^2} \right) + \sqrt{\left(\frac{1}{c_T^2} - \frac{1}{c_R^2} \right)^2 + \frac{4A\rho}{\omega^2 EI}} \right], \tag{19}$$

$$\lambda_2^{\beta=0} = -\frac{\omega^2}{2} \left[\left(\frac{1}{c_T^2} + \frac{1}{c_R^2} \right) - \sqrt{\left(\frac{1}{c_T^2} - \frac{1}{c_R^2} \right)^2 + \frac{4A\rho}{\omega^2 EI}} \right]. \tag{20}$$

Here, $\lambda_1^{\beta=0}$ is strictly negative, whereas $\lambda_2^{\beta=0}$ changes its sign for a certain angular frequency $\tilde{\omega}^{\beta=0}$:

$$\sqrt{\left(\frac{1}{c_T^2}-\frac{1}{c_R^2}\right)^2+\frac{4A}{\tilde{\omega}^2 I c_R^2}}=\frac{1}{c_T^2}+\frac{1}{c_R^2}, \tag{21}$$

with

$$\left(\tilde{\omega}^{\beta=0}\right)^2=c_T^2\frac{A}{I}=\frac{\kappa GA}{\rho I}. \tag{22}$$

This characteristic frequency is identical to $\tilde{\omega}_2$ derived above for an infinite Timoshenko beam on elastic Winkler foundation. Since the solution (7) in the space-domain is related to $\sqrt{\lambda}$, a change of the sign of a real value $\lambda_2 \in \mathbb{R}$ influences the character of the solution significantly. The properties of λ_1, λ_2 with respect to the characteristic frequencies $\tilde{\omega}_1$, $\tilde{\omega}_2$ are summarized in the following equation:

$$\begin{aligned}&\tilde{\omega}_1=\sqrt{\tfrac{\beta}{\rho A}},\\ &\tilde{\omega}_2=\sqrt{\tfrac{\kappa GA}{\rho I}};\end{aligned}\qquad \begin{cases}\omega<\tilde{\omega}_1 & : \quad \lambda_{1,2}=a\pm \mathrm{i}b; \quad a,b\in\mathbb{R}.\\ \omega=\tilde{\omega}_1 & : \quad \lambda_1=0, \quad \lambda_2=-\dfrac{\beta}{EA}.\\ \tilde{\omega}_1<\omega<\tilde{\omega}_2 & : \quad \lambda_1,\lambda_2\in\mathbb{R}; \quad \lambda_1>0, \quad \lambda_2<0.\\ \omega=\tilde{\omega}_2 & : \quad \lambda_2\in\mathbb{R}, \quad \lambda_1=0, \quad \lambda_2<0.\\ \omega>\tilde{\omega}_2 & : \quad \lambda_1,\lambda_2\in\mathbb{R}; \quad \lambda_1<0, \quad \lambda_2<0.\end{cases} \tag{23}$$

In order to derive dynamic stiffness relationships, the normalized deformation $w_F(x,\xi)$ due to a unit force $\hat{F}=1$[N]acting at the point ξ in an arbitrary distance r, $r=|x-\xi|$, to the point of observation, and the normalized rotation $\varphi_M(x,\xi)$ due to a unit moment $\hat{M}=1$[Nm] at ξ are required. For this purpose, a short operator notation of the governing differential equations (6) in the frequency-domain as used by Antes in Ref. [16] is beneficial.

$$\mathbf{B}_s\begin{bmatrix}\hat{w}\\ \hat{\varphi}\end{bmatrix}=\begin{bmatrix}\kappa GA\dfrac{\partial^2}{\partial x^2}-M_{T\beta} & \kappa GA\dfrac{\partial}{\partial x}\\ -\kappa GA\dfrac{\partial}{\partial x} & EI\dfrac{\partial^2}{\partial x^2}-\kappa GA-M_R\end{bmatrix}\begin{bmatrix}\hat{w}\\ \hat{\varphi}\end{bmatrix}=-\begin{bmatrix}\hat{q}\\ \hat{m}\end{bmatrix}. \tag{24}$$

According to Antes [16] the problem of finding the fundamental solutions can be reduced to determining a scalar function ψ which fulfills Eq. (25) incorporating the determinant of the operator matrix $\mathbf{B}_s$.

$$\det(\mathbf{B}_s)\,\psi=-\delta(x-\xi). \tag{25}$$

The solution of Eq. (25) is given in Refs. [16,23] as

$$\psi=\frac{1}{2\kappa GAEI(\lambda_1-\lambda_2)}\left[\frac{\mathrm{e}^{-\sqrt{\lambda_1}r}}{\sqrt{\lambda_1}}-\frac{\mathrm{e}^{-\sqrt{\lambda_2}r}}{\sqrt{\lambda_2}}\right]. \tag{26}$$

Here, λ_1 and λ_2 are the two roots of $\det(\mathbf{B}_s)=0$ derived above (Eqs. (11)–(13)). Finally, the fundamental solutions are found using the matrix of cofactors $\mathbf{B}_s^{\mathrm{co}}$ of $\mathbf{B}_s$ with $\mathbf{B}_s^{\mathrm{co}}=\det(\mathbf{B}_s)\mathbf{B}_s^{-1}$.

$$\begin{bmatrix}w_F & w_M\\ \varphi_F & \varphi_M\end{bmatrix}=\mathbf{B}_s^{\mathrm{co}}\psi=\begin{bmatrix}EI\dfrac{\partial^2}{\partial x^2}-\kappa GA-M_R & -\kappa GA\dfrac{\partial}{\partial x}\\ \kappa GA\dfrac{\partial}{\partial x} & \kappa GA\dfrac{\partial^2}{\partial x^2}-M_{T\beta}\end{bmatrix}\psi. \tag{27}$$

In Eq. (27) the symbols w_M and φ_F denote the vertical deformation due to a unit moment and the rotation due to a unit force acting at the point ξ, respectively. Evaluating Eq. (27), the desired normalized deformation w_F and rotation

φ_M are obtained as:

$$w_F = \frac{1}{2\kappa GA(\lambda_1-\lambda_2)}\left[\frac{\mathrm{e}^{-\sqrt{\lambda_1}r}}{\sqrt{\lambda_1}}\left(\lambda_1-\frac{\kappa GA+M_R}{EI}\right)-\frac{\mathrm{e}^{-\sqrt{\lambda_2}r}}{\sqrt{\lambda_2}}\left(\lambda_2-\frac{\kappa GA+M_R}{EI}\right)\right], \tag{28}$$

$$\varphi_M = \frac{1}{2EI(\lambda_1-\lambda_2)}\left[\frac{\mathrm{e}^{-\sqrt{\lambda_1}r}}{\sqrt{\lambda_1}}\left(\lambda_1-\frac{M_{T\beta}}{\kappa GA}\right)-\frac{\mathrm{e}^{-\sqrt{\lambda_2}r}}{\sqrt{\lambda_2}}\left(\lambda_2-\frac{M_{T\beta}}{\kappa GA}\right)\right]. \tag{29}$$

For a more detailed description of the underlying operator theory the reader is referred to Ref. [24, Part II, Chapter 3].

It should be noted that the square roots $\sqrt{\lambda_1}$, $\sqrt{\lambda_2}$ are ambiguous. For physical reasons, these values have to be chosen as follows:

$$\tilde{\omega}_1=\sqrt{\frac{\beta}{\rho A}},\qquad \tilde{\omega}_2=\sqrt{\frac{\kappa GA}{\rho I}};\qquad \begin{cases}\omega<\tilde{\omega}_1 & : \ \Re\{\sqrt{\lambda_1}\}>0,\ \Re\{\sqrt{\lambda_2}\}>0,\\ \tilde{\omega}_1\leqslant\omega<\tilde{\omega}_2 & : \ \Re\{\sqrt{\lambda_1}\}>0,\ \Im\{\sqrt{\lambda_2}\}>0,\\ \omega\geqslant\tilde{\omega}_2 & : \ \Im\{\sqrt{\lambda_1}\}>0,\ \Im\{\sqrt{\lambda_2}\}>0.\end{cases} \tag{30}$$

Due to $K_F=\hat{F}/\hat{w}$ and $K_M=\hat{M}/\hat{\varphi}$ at the point $r=0$ where $\hat{F}$ and $\hat{M}$ act onto the beam, the stiffnesses K_F, K_M follow directly from solutions (28) and (29), respectively.

$$w_F(r=0,t)=\hat{w}_0\mathrm{e}^{\mathrm{i}\omega t},\quad \varphi_M(r=0,t)=\hat{\varphi}_0\mathrm{e}^{\mathrm{i}\omega t}, \tag{31}$$

$$K_F=\frac{1}{\hat{w}_0}=\frac{2\kappa GA(\lambda_1-\lambda_2)\sqrt{\lambda_1\lambda_2}}{\sqrt{\lambda_2}\left(\lambda_1-\frac{\kappa GA+M_R}{EI}\right)-\sqrt{\lambda_1}\left(\lambda_2-\frac{\kappa GA+M_R}{EI}\right)}, \tag{32}$$

$$K_M=\frac{1}{\hat{\varphi}_0}=\frac{2EI(\lambda_1-\lambda_2)\sqrt{\lambda_1\lambda_2}}{\sqrt{\lambda_2}\left(\lambda_1-\frac{M_{T\beta}}{\kappa GA}\right)-\sqrt{\lambda_1}\left(\lambda_2-\frac{M_{T\beta}}{\kappa GA}\right)}. \tag{33}$$

Below the first critical frequency $\tilde{\omega}_1$ both stiffnesses K_F and K_M are purely real-valued and indicate properties of a corresponding frequency-dependent spring. Thus, $\tilde{\omega}_1$ is a cutoff frequency, where wave propagation starts to exist. Above the second critical frequency $\tilde{\omega}_2$ the stiffnesses K_F and K_M are purely imaginary and indicate radiation damping which can be described by a constant damping coefficient d when ω tends towards infinity:

$$\lim_{\omega\to\infty}K_F=K_F^{\infty}=\frac{2\kappa GA}{c_T}\,\mathrm{i}\omega=2A\sqrt{\kappa G\rho}\mathrm{i}\omega, \tag{34}$$

$$\lim_{\omega\to\infty}K_M=K_M^{\infty}=\frac{2EI}{c_R}\,\mathrm{i}\omega=2I\sqrt{E\rho}\mathrm{i}\omega. \tag{35}$$

For the vertical degree of freedom, the relationship to viscous damping with the corresponding force,

$$F(t)=d\dot{w}(t), \tag{36}$$

in the time-domain follows directly from the assumption of a time-harmonic behaviour of both quantities, $w(t)$ as well as $F(t)$:

$$F(t)=\hat{F}\mathrm{e}^{\mathrm{i}\omega t};\quad w(t)=\hat{w}\mathrm{e}^{\mathrm{i}\omega t}. \tag{37}$$

Thus, Eq. (36) in the time-domain corresponds to

$$\hat{F}=\mathrm{i}\omega d\hat{w} \tag{38}$$

in the frequency domain. Comparing Eqs. (34) and (38) yields a constant damping coefficient $d=2A\sqrt{\kappa G\rho}$ in case of the translational stiffness for ω tending towards infinity.

2.2. Infinite Euler–Bernoulli beam

The governing differential equation of an infinite Euler–Bernoulli beam on elastic Winkler foundation of stiffness $\beta\,[\mathrm{N/m^2}]$,

$$EI\,\frac{\partial^4}{\partial x^4}w(x,t)+\beta w(x,t)+\rho A\ddot{w}(x,t)=0 \tag{39}$$

is solved by exponential functions $w(x,t)=\hat{w}\mathrm{e}^{\lambda x}\mathrm{e}^{\mathrm{i}\omega t}$. The dynamic stiffnesses K_F and K_M are derived in Ref. [18]:

$$K_F=8EIW^3, \tag{40}$$

$$K_M=4EIW, \tag{41}$$

$$W=\frac{1}{2}\sqrt[4]{\frac{\beta}{EI}}\times\begin{cases}\sqrt{2}\sqrt[4]{1-\eta^2} & \text{for } \eta^2\leqslant 1\\ (1+\mathrm{i})\sqrt[4]{\eta^2-1} & \text{for } \eta^2>1.\end{cases},\quad \eta^2=\omega^2\frac{\rho A}{\beta}. \tag{42}$$

The dimensionless frequency used in Eq. (42) is identical to that defined for the Timoshenko beam in Eq. (10). As for the Timoshenko beam, $\eta=1.0$ corresponds to the cutoff frequency $\tilde{\omega}_1$, where wave propagation occurs for the first time. Thus, K_F and K_M given in Eqs. (40) and (41), respectively, are purely real-valued for $\omega<\tilde{\omega}_1$. However, there is no equivalent to the second characteristic frequency $\tilde{\omega}_2$ of the Timoshenko beam. Evaluating the limit of Eqs. (40) and (41) for $\eta\to\infty$, the following asymptotic dynamic stiffness coefficients for high frequency can be derived [18,19]:

$$\lim_{\omega\to\infty}K_F=K_F^{\infty}=2\sqrt{2}EIC^{3/4}(\mathrm{i}\omega)^{3/2}, \tag{43}$$

$$\lim_{\omega\to\infty}K_M=K_M^{\infty}=2\sqrt{2}EIC^{1/4}(\mathrm{i}\omega)^{1/2},\quad C=\frac{\rho A}{EI}. \tag{44}$$

It is important to note that Eqs. (43) and (44) contain rational powers of the frequency. This is in contrast to the linear frequency dependence obtained for the Timoshenko beam in Eqs. (34) and (35). In the special case of vanishing Winkler foundation, $\beta=0$, the dynamic stiffness coefficients are identical to the asymptotic values given in Eqs. (43), (44) [19] throughout the complete frequency range:

$$\beta=0:\quad K_F^{\beta=0}=\lim_{\omega\to\infty}K_F^{\beta\neq 0},\quad K_M^{\beta=0}=\lim_{\omega\to\infty}K_M^{\beta\neq 0}. \tag{45}$$

3. Time-domain models of infinite beams

The dynamic stiffnesses given in Eqs. (32), (33) and (40), (41) completely describe the relationship between the amplitudes $\hat{F}_0$, $\hat{M}_0$ of a point load or moment, respectively and the resulting deformations $\hat{w}_0$, $\hat{\varphi}_0$ at $x=0$ in the frequency-domain. Based on these equations, the response of the Timoshenko or Euler–Bernoulli beam to transient excitations could be obtained using inverse Fourier transformation and the convolution theorem. However, the numerical evaluation of the associated convolution integrals is computationally expensive. Therefore, direct time-domain models are more desirable for the analysis of transient dynamic problems. In this paper, the latter are obtained using the so-called mixed-variables technique [20]. This technique is based on a rational approximation of the low-frequency dynamic stiffness $K-K^{\infty}$,

$$\hat{F}_0=K_F(\mathrm{i}\omega)\hat{w}_0=K_F^{\infty}\hat{w}_0+(K_F-K_F^{\infty})\hat{w}_0, \tag{46}$$

$$\hat{M}_0=K_M(\mathrm{i}\omega)\hat{\varphi}_0=K_M^{\infty}\hat{\varphi}_0+(K_M-K_M^{\infty})\hat{\varphi}_0, \tag{47}$$

using a least-squares approach. The resulting rational function can be transformed into a system of linear equations in the frequency-domain by means of an algebraic splitting process using internal variables. The resulting system of linear equations with respect to $\mathrm{i}\omega$ corresponds to a system of first-order differential

equations in the time-domain. The mixed-variables technique is described in detail in Ref. [26]. The essential steps of the frequency-to-time transformation of Eqs. (46)–(47) are summarized briefly in the following:

Step 1: Strictly proper rational approximation of low-frequency dynamic stiffness $K - K^{\infty}$:

$$K_F - K_F^{\infty} \approx \frac{P_0 + (\mathrm{i}\omega)P_1 + \cdots + (\mathrm{i}\omega)^{M-1}P_{M-1}}{1 + (\mathrm{i}\omega)Q_1 + \cdots + (\mathrm{i}\omega)^{M}Q_M} = \frac{P(\mathrm{i}\omega)}{Q(\mathrm{i}\omega)}, \tag{48}$$

$$K_M - K_M^{\infty} \approx \frac{p_0 + (\mathrm{i}\omega)p_1 + \cdots + (\mathrm{i}\omega)^{M-1}p_{M-1}}{1 + (\mathrm{i}\omega)q_1 + \cdots + (\mathrm{i}\omega)^{M}q_M} = \frac{p(\mathrm{i}\omega)}{q(\mathrm{i}\omega)}. \tag{49}$$

The rational approximation is equivalent to an alternative Padé series expansion as has been used for example by Song [28].

$$\frac{P(\mathrm{i}\omega)}{Q(\mathrm{i}\omega)} = \frac{(\mathrm{i}\omega)^{-1}P_{M-1} + \cdots + (\mathrm{i}\omega)^{-(M-1)}P_1 + (\mathrm{i}\omega)^{-M}P_0}{Q_M + \cdots + (\mathrm{i}\omega)^{-(M-1)}Q_1 + (\mathrm{i}\omega)^{-M}}. \tag{50}$$

The degree of rational approximation M can be chosen arbitrarily. In previous publications [18,19,26], accurate results have been obtained with $M = 5$ already. The coefficients P_j, Q_j and p_j, q_j are calculated minimizing the error-norms E_F, E_M:

$$E_F = \sum_{j=1}^{s} \| Q(\mathrm{i}\omega_j)[K_F(\omega_j) - K_F^{\infty}(\omega_j)] - P(\mathrm{i}\omega_j)\|,$$

$$E_M = \sum_{j=1}^{s} \| q(\mathrm{i}\omega_j)[K_M(\omega_j) - K_M^{\infty}(\omega_j)] - p(\mathrm{i}\omega_j)\|, \tag{51}$$

using an amount of $s+1$ distinct values $\omega_j = j\Delta\omega$, $j = 1, \ldots, s$ with a frequency increment $\Delta\omega$.

Step 2: Replacement of the fraction $P(\mathrm{i}\omega)/Q(\mathrm{i}\omega)$ by a new state variable $\hat{v}_1$ and changing from the proper fraction $P(\mathrm{i}\omega)/Q(\mathrm{i}\omega)$ to the improper fraction $Q(\mathrm{i}\omega)/P(\mathrm{i}\omega)$ (here and in the following only the vertical degree of freedom is addressed for conciseness):

$$\hat{F}_0 = \frac{P(\mathrm{i}\omega)}{Q(\mathrm{i}\omega)}\hat{w}_0 + K_F^{\infty}\hat{w}_0 = \hat{v}_1 + K_F^{\infty}\hat{w}_0,$$

$$\hat{v}_1 = \frac{P(\mathrm{i}\omega)}{Q(\mathrm{i}\omega)}\,\hat{w}_0 \quad \rightarrow \hat{w}_0 = \frac{Q(\mathrm{i}\omega)}{P(\mathrm{i}\omega)}\,\hat{v}_1,$$

$$\hat{v}_1 : \text{first internal variable.} \tag{52}$$

Step 3: Splitting of $Q(\mathrm{i}\omega)/P(\mathrm{i}\omega)$ into a linear function with respect to $\mathrm{i}\omega$ and a strictly proper remainder $R^{(0)}(\mathrm{i}\omega)/P(\mathrm{i}\omega)$ by means of a comparison of coefficients; introduction of a second internal variable $\hat{v}_2$ to replace the remainder $R^{(0)}(\mathrm{i}\omega)/P(\mathrm{i}\omega)$:

$$\frac{Q(\mathrm{i}\omega)}{P(\mathrm{i}\omega)} = S_0^{(0)} + \mathrm{i}\omega S_1^{(0)} + \frac{R^{(0)}(\mathrm{i}\omega)}{P(\mathrm{i}\omega)}, \quad \frac{R^{(0)}(\mathrm{i}\omega)}{P(\mathrm{i}\omega)} : \text{proper fraction} \tag{53}$$

$$R^{(0)}(\mathrm{i}\omega) = R_0^{(0)} + \mathrm{i}\omega R_1^{(0)} + (\mathrm{i}\omega)^2 R_2^{(0)} + \cdots (\mathrm{i}\omega)^{M-2} R_{M-2}^{(0)}, \tag{54}$$

$$\hat{w}_0 = (S_0^{(0)} + \mathrm{i}\omega S_1^{(0)})\hat{v}_1 + \hat{v}_2, \tag{55}$$

$$\hat{v_2} = \frac{R^{(0)}(\mathrm{i}\omega)}{P(\mathrm{i}\omega)}\,\hat{v}_1 \tag{56}$$

$$\rightarrow \hat{v}_1 = \frac{P(\mathrm{i}\omega)}{R^{(0)}(\mathrm{i}\omega)}\,\hat{v}_2, \quad \frac{P(\mathrm{i}\omega)}{R^{(0)}(\mathrm{i}\omega)} : \text{improper fraction}, \tag{57}$$

$$\hat{v}_2 : \text{second internal variable.} \tag{58}$$

Further steps: Continuation of step 3 until the rational function has been completely replaced by linear equations. A total of M internal variables is introduced during this process, where M is the degree of rational

approximation. The following representation of the force–displacement relationship is obtained:

$$\begin{bmatrix} 0 & 1 & 0 & \cdots & 0 \\ 1 & -S_0^{(0)} & -1 & \cdots & 0 \\ 0 & -1 & S_0^{(1)} & \cdots & 0 \\ \vdots & \vdots & \vdots & \vdots & \vdots \\ 0 & 0 & \cdots & \mp 1 & \pm S_0^{(M-1)} \end{bmatrix} \begin{bmatrix} \hat{w}_0 \\ \hat{v}_1 \\ \hat{v}_2 \\ \vdots \\ \hat{v}_M \end{bmatrix} + \mathrm{i}\omega \begin{bmatrix} 0 & 0 & 0 & \cdots & 0 \\ 0 & -S_1^{(0)} & 0 & \cdots & 0 \\ 0 & 0 & S_1^{(1)} & \cdots & 0 \\ \vdots & \vdots & \vdots & \ddots & \vdots \\ 0 & 0 & 0 & \cdots & \pm S_1^{(M-1)} \end{bmatrix} \begin{bmatrix} \hat{w}_0 \\ \hat{v}_1 \\ \hat{v}_2 \\ \vdots \\ \hat{v}_M \end{bmatrix} + \begin{bmatrix} K^{\infty} \hat{w}_0 \\ 0 \\ 0 \\ \vdots \\ 0 \end{bmatrix} = \begin{bmatrix} \hat{F}_0 \\ 0 \\ 0 \\ \vdots \\ 0 \end{bmatrix}. \tag{59}$$

Assuming a harmonic behaviour of the state variables,

$$\mathbf{z}(t) = \hat{\mathbf{z}} \mathrm{e}^{\mathrm{i}\omega t}, \quad \mathbf{r}(t) = \hat{\mathbf{r}} \mathrm{e}^{\mathrm{i}\omega t}, \tag{60}$$

the factor $\mathrm{i}\omega$ in Eq. (59) can be interpreted as a first-order time derivative. However, in order to derive a time-domain equivalent of Eq. (59), an interpretation of the asymptotic part $K^{\infty}\hat{w}$ is necessary. Here differences occur for the Timoshenko and Euler–Bernoulli beam, respectively, as is shown in the following.

3.1. Timoshenko beam: interpretation of asymptotic dynamic stiffness

Here, both the vertical and rotational asymptotic dynamic stiffness given in Eqs (34) and (35), respectively, follow linear functions of $\mathrm{i}\omega$ and can thus be interpreted as viscous dashpots in the time domain. Including the corresponding coefficients K_F^{∞} and K_M^{∞} at the position (1,1) of the second matrix in Eq. (59), the latter corresponds to a first-order differential equation with respect to time:

$$\mathbf{A}\mathbf{z}(t) + \mathbf{B}\dot{\mathbf{z}}(t) = \mathbf{r}(t), \tag{61}$$

with

$$\mathbf{B} = \mathrm{diag}\left\{ \frac{2\kappa GA}{c_T} \quad -S_1^{(0)} \quad S_1^{(1)} \quad \cdots \quad \pm S_1^{(M-1)} \right\}, \tag{62}$$

$$\mathbf{z}^{\mathrm{T}}(t) = \begin{bmatrix} w_0(t) & v_1(t) & \cdots & v_M(t) \end{bmatrix}, \quad \mathbf{r}^{\mathrm{T}}(t) = \begin{bmatrix} F_0(t) & 0 & \cdots & 0 \end{bmatrix} \tag{63}$$

for the vertical degree of freedom and

$$\mathbf{B} = \mathrm{diag}\left\{ \frac{2EI}{c_R} \quad -S_1^{(0)} \quad S_1^{(1)} \quad \cdots \quad \pm S_1^{(M-1)} \right\}, \tag{64}$$

$$\mathbf{z}^{\mathrm{T}}(t) = \begin{bmatrix} \varphi_0(t) & v_1(t) & \cdots & v_M(t) \end{bmatrix}, \quad \mathbf{r}^{\mathrm{T}}(t) = \begin{bmatrix} M_0(t) & 0 & \cdots & 0 \end{bmatrix} \tag{65}$$

for the rotational degree of freedom. The matrix $\mathbf{A}$ is the first matrix of Eq. (59). The ordinary differential equation (61) can be coupled to finite element models of additional structural members (even with nonlinear behaviour) and solved in the time-domain using standard numerical time-stepping schemes.

3.2. Euler–Bernoulli beam: interpretation of asymptotic dynamic stiffness

In contrast to the Timoshenko beam, the high-frequency asymptotic dynamic stiffness coefficients of the Euler–Bernoulli beam given in Eqs. (43) and (44) contain rational powers of $\mathrm{i}\omega$. Nevertheless, the harmonic behaviour

$$\mathbf{z}(x,t)=\begin{bmatrix} w(x,t)\\ \varphi(x,t)\end{bmatrix}=\begin{bmatrix} w(x)\\ \varphi(x)\end{bmatrix}\mathrm{e}^{\mathrm{i}\omega t},\quad \frac{\partial^m}{\partial t^m}\,\mathbf{z}(x,t)=(\mathrm{i}\omega)^m\mathbf{z}(x,t), \tag{66}$$

can be used to transform the asymptotic frequency-domain descriptions (43), (44) for the infinite Euler–Bernoulli beam into the time domain. F_0^∞ and M_0^∞ are those parts of the interaction force and moment, respectively, which correspond to the high-frequency asymptotic behaviour.

$$\hat{F}_0=\frac{P(\mathrm{i}\omega)}{Q(\mathrm{i}\omega)}\,\hat{w}_0+\hat{F}_0^\infty,\quad \hat{M}_0=\frac{p(\mathrm{i}\omega)}{q(\mathrm{i}\omega)}\,\hat{\varphi}_0+\hat{M}_0^\infty,$$

$$\hat{F}_0^\infty=K_F^\infty\hat{w}_0,\quad \hat{M}_0^\infty=K_M^\infty\hat{\varphi}_0,$$

$$F_0^\infty(t)=2\sqrt{2}EIC^{3/4}[{}_{-\infty}D_t^{3/2}w_0(t)],\quad C=\frac{\rho A}{EI}, \tag{67}$$

$$M_0^\infty(t)=2\sqrt{2}EIC^{1/4}[{}_{-\infty}D_t^{1/2}\varphi_0(t)]. \tag{68}$$

Here, noninteger powers of $(\mathrm{i}\omega)$ are interpreted as fractional derivatives of the unknown displacement $w_0(t)$ and rotation $\varphi_0(t)$, respectively. This is based on the so-called Riemann–Liouville definition (69) of fractional differentiation which can be found in the textbook [25], for example.

$${}_aD_t^\nu\mathbf{z}=\frac{1}{\Gamma(m-\nu)}\frac{\mathrm{d}^m}{\mathrm{d}t^m}\int_a^t\frac{\mathbf{z}(\tau)}{(t-\tau)^{\nu+1-m}}\,\mathrm{d}\tau,\quad m-1\leqslant\nu\leqslant m. \tag{69}$$

In Eq. (69), m is an integer number. Application of definition (69) using the lower terminal $a=-\infty$ to a harmonic function returns the latter together with a factor $(\mathrm{i}\omega)^\nu$.

$${}_{-\infty}D_t^\nu\mathrm{e}^{\mathrm{i}\omega t}=(\mathrm{i}\omega)^\nu\mathrm{e}^{\mathrm{i}\omega t}. \tag{70}$$

However, if the quantities $\mathbf{z}$ between $(t\to-\infty)$ and $t=0$, where the system starts to exist, are identically zero, then the lower limit of the integral in Eq. (69) can be replaced by 0:

$$\mathbf{z}(t)\equiv\mathbf{0}\quad\text{for}\quad -\infty<t\leqslant 0. \tag{71}$$

$$\to{}_{-\infty}D_t^\nu\mathbf{z}=\frac{1}{\Gamma(m-\nu)}\frac{\partial^m}{\partial t^m}\int_0^t\frac{\mathbf{z}(\tau)}{(t-\tau)^{\nu+1-m}}\,\mathrm{d}\tau,\quad m-1\leqslant\nu\leqslant m.$$

Thus, the approach presented in this paper is limited to situations with zero initial conditions for the displacements and rotations. An initial impact $I_0=mv_0$ can be modelled by applying a constant force within a very short time interval h: $I_0=Fh$. Using the above interpretation given in Eqs. (67) and (68), the frequency-domain representation (59) corresponds to the following system of fractional differential equations in the time-domain:

$$\mathbf{A}\mathbf{z}(t)+\mathbf{B}_E\dot{\mathbf{z}}(t)+\mathbf{C}_\nu[{}_{-\infty}D_t^\nu\mathbf{z}(t)]=\mathbf{r}(t), \tag{72}$$

with

$$\nu=\tfrac{3}{2},\quad \mathbf{C}_{3/2}=\mathrm{diag}\left\{2\sqrt{2}EIC^{\frac{3}{4}}\ \ 0\ \ \cdots\ \ 0\right\}, \tag{73}$$

$$\mathbf{z}^{\mathrm{T}}(t)=[w_0(t)\ \ v_1(t)\ \ \cdots\ \ v_M(t)],\quad \mathbf{r}^{\mathrm{T}}(t)=[F_0(t)\ \ 0\ \ \cdots\ \ 0]$$

for the vertical degree of freedom and

$$\nu=\tfrac{1}{2},\quad \mathbf{C}_{1/2}=\mathrm{diag}\left\{\,2\sqrt{2}EIC^{\frac{1}{4}}\quad 0\quad\cdots\quad 0\,\right\}, \tag{74}$$

$$\mathbf{z}^{\mathrm{T}}(t) = [\varphi_0(t)\ \ v_1(t)\ \ \cdots\ \ v_M(t)], \quad \mathbf{r}^{\mathrm{T}}(t) = [M_0(t)\ \ 0\ \ \cdots\ \ 0]$$

for the rotational degree of freedom. The matrix $\mathbf{A}$ is the same as for the Timoshenko beam. $\mathbf{B}_E$ is given in Eq. (75).

$$\mathbf{B}_E = \mathrm{diag}\left\{0\ \ -S_1^{(0)}\ \ S_1^{(1)}\ \ \cdots\ \ \pm S_1^{(M-1)}\right\}. \tag{75}$$

The system of fractional differential equations (72) can be solved numerically using a specific time-stepping scheme [27,26] developed for this purpose. In comparison to the first-order differential equation (61), the numerical effort increases due to the evaluation of memory integrals.

Finally, it should be noted that in the special case of vanishing Winkler foundation, $\beta = 0$, the force–displacement relationships of the Euler–Bernoulli beam are described by rational functions of $\mathrm{i}\omega$ throughout the complete frequency range (see Eqs. (43)–(45)). In this case, there is no need to apply the mixed-variables technique. The following scalar fractional differential equations describe the force–displacement- and moment–rotation-relationship of an infinite Euler–Bernoulli beam with $\beta = 0$ in the time-domain:

$$\left.\begin{aligned} F_0(t) &= 2\sqrt{2}EIC^{3/4}[{}_{-\infty}D_t^{3/2}w_0(t)] \\ M_0(t) &= 2\sqrt{2}EIC^{1/4}[{}_{-\infty}D_t^{1/2}\varphi_0(t)] \end{aligned}\right\} \quad \text{if } \beta = 0. \tag{76}$$

4. Example

In order to illustrate the differences between the Timoshenko and Euler–Bernoulli beam models a specific system with material data given in Eq. (77) has been analysed.

$$\begin{aligned} &E = 2.1 \times 10^{11}\,[\mathrm{N/m^2}], \quad I = 3055\,[\mathrm{cm^4}], \\ &\nu = 0.3, \quad \beta = 4.375 \times 10^6\,[\mathrm{N/m^2}], \\ &A = 7686\ [\mathrm{mm^2}], \quad \rho A = 60.34\ [\mathrm{kg/m}], \quad \kappa = \tfrac{5}{6}. \end{aligned} \tag{77}$$

The vertical dynamic stiffnesses derived for the Timoshenko and Euler–Bernoulli beam on elastic foundation in Eqs. (32) and (40), respectively are shown in Fig. 3. As described in Section 2.1, the infinite Timoshenko beam is characterized by two frequencies,

$$\tilde{\omega}_1 = \sqrt{\frac{\beta}{\rho A}} = 269.3\,\frac{1}{\mathrm{s}}, \quad \tilde{\omega}_2 = \sqrt{\frac{\kappa GA}{\rho I}} = 46445.3\,\frac{1}{\mathrm{s}}. \tag{78}$$

The low-frequency range is shown in Fig. 3a. Here, a very good agreement between the dynamic stiffness of Timoshenko's beam and Euler–Bernoulli's beam can be seen. As expected, the imaginary part of the vertical stiffness vanishes for $\omega < \tilde{\omega}_1$ in both cases. As explained in Section 2.2, the cutoff-frequencies of Timoshenko and Euler–Bernoulli beam are identical. However, the agreement between the stiffness curves corresponding to the two different beam models is restricted to the low-frequency range, as can be seen in Fig. 3b. As described in Section 2.1, the real part of the dynamic stiffness of the Timoshenko beam vanishes for excitation frequencies bigger than $\tilde{\omega}_2$. This is not the case for the Euler–Bernoulli beam. The imaginary parts corresponding to the two different beam models agree reasonably for $\omega < \tilde{\omega}_2$. However, the stiffness curves differ strongly for large frequencies. Recall that the asymptotic dynamic stiffness follows a linear function of $\mathrm{i}\omega$ in case of the Timoshenko beam whereas a rational power $(\mathrm{i}\omega)^{3/2}$ is involved in case of the Euler–Bernoulli beam (Fig. 3).

The calculation in the time-domain is demonstrated using the example system shown in Fig. 2. Here, the Winkler foundation is replaced by a single spring of stiffness k at $x = 0$ with

$$k = 5.0 \times 10^8\,\mathrm{N/m}. \tag{79}$$

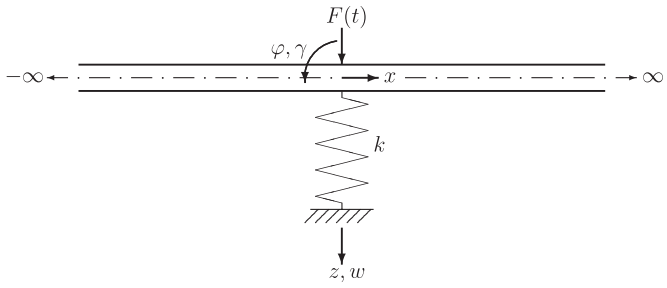

Fig. 2. Infinite beam supported by a single spring at $x = 0$.

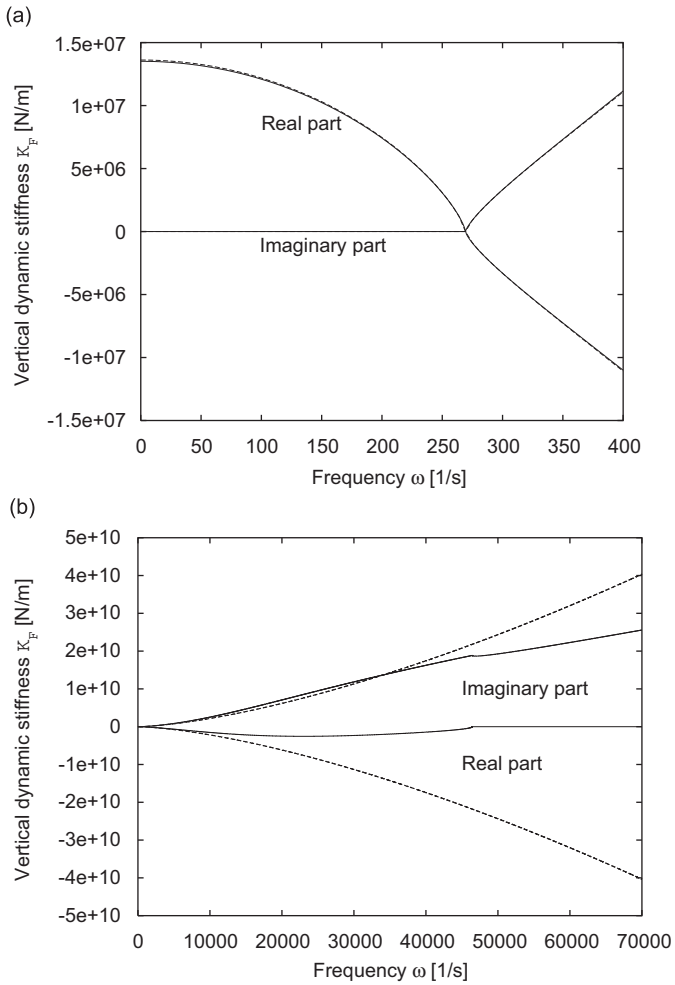

Fig. 3. Vertical dynamic stiffness for the Timoshenko and Euler–Bernoulli beam models on elastic Winkler foundation: (a) low-frequency range, (b) frequency-range 0–70,000 $\frac{1}{s}$. ——— Timoshenko beam, – – – – Euler–Bernoulli beam.

In order to obtain a time-domain model, the low-frequency part of the vertical dynamic stiffness of the Timoshenko beam is approximated by the ratio of two polynomials (Eq. (48)) as described in Section 3. As an example, the coefficients P_i, Q_i of a rational approximation of degree $M = 5$ and $S_0^{(i)}, S_1^{(i)}$ of the equivalent system of linear equations are given in Table 1. The agreement between the exact low-frequency vertical

Table 1
Rational approximation of the low-frequency part of the vertical dynamic stiffness of a Timoshenko beam

i	P_{i-1}	Q_i	$S_0^{(i-1)}$	$S_1^{(i-1)}$
1	0	0.14276E − 03	+0.96198E − 10	−0.20802E − 13
2	−2.4059E + 05	6.00998E − 09	−0.13731E + 10	−0.38614E + 05
3	−7.0732	1.95476E − 13	+0.42453E − 09	+0.38183E − 13
4	−0.1515E − 03	2.91726E − 18	+0.18656E + 09	+0.16073E + 05
5	−2.4293E − 09	5.05336E − 23	+0.32199E − 09	+0.79140E − 13

Material data according to Eq. (77). $M = 5$, Input range: $\omega_0 = 0$, $\omega_{\text{end}} = 80,000\,1/\text{s}$, frequency increment $\Delta\omega = 100\,1/\text{s}$.

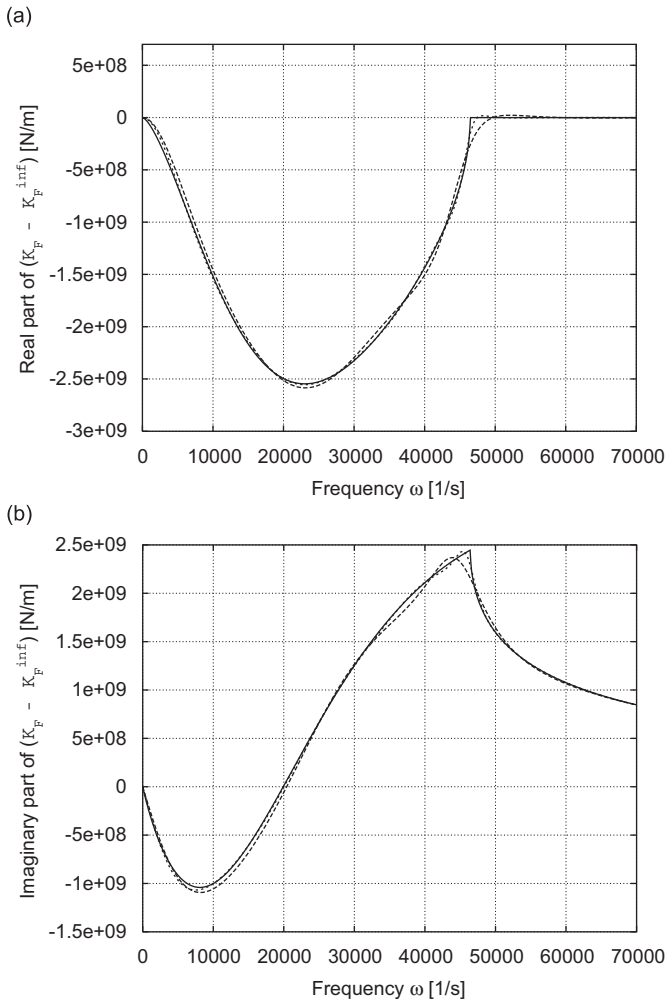

Fig. 4. Low-frequency part of the vertical dynamic stiffness of the Timoshenko beam: (a) real part, (b) imaginary part. ——— exact: $K_F - K_F^\infty$, K_F according to Eq. (32), K_F^∞ according to Eq. (34), — — — — $M = 5$, - - - - - - $M = 7$.

dynamic stiffness coefficient and rational approximations of degree $M = 5$ and 7 is shown in Fig. 4. Using the rational stiffness approximation, the vertical displacement at the point of excitation of the coupled beam–spring system shown in Fig. 2 is described by the following system of first-order differential equations:

$$\tilde{\mathbf{A}}\mathbf{z}(t) + \mathbf{B}\dot{\mathbf{z}}(t) = \mathbf{r}(t), \tag{80}$$

with

$$\tilde{\mathbf{A}} = \begin{bmatrix} k & 1 & 0 & \cdots & 0 \\ 1 & -S_0^{(0)} & -1 & \cdots & 0 \\ 0 & -1 & S_0^{(1)} & \cdots & 0 \\ \vdots & \vdots & \vdots & \vdots & \vdots \\ 0 & 0 & \cdots & \mp 1 & \pm S_0^{(M-1)} \end{bmatrix}, \quad \mathbf{z}(t) = \begin{bmatrix} w_0(t) \\ v_1(t) \\ v_2(t) \\ \vdots \\ v_M(t) \end{bmatrix}. \tag{81}$$

Here, the spring stiffness k has been included at the position (1,1) of the matrix $\tilde{\mathbf{A}}$. The right-hand side vector $\mathbf{r}$ and the matrix $\mathbf{B}$ are given in Eqs. (62) and (63), respectively. Using Eq. (80), the vertical displacement $w(x=0,t) = w_0(t)$ due to a transient unit-impulse load,

$$i_r = \int_0^{h_0} F_0(t)\,\mathrm{d}t = 1.0\,[\mathrm{Nm}], \quad h_0 = 10^{-6}\,\mathrm{s}, \tag{82}$$

acting within the time-interval $0 \leqslant t \leqslant h_0$ has been computed. The numerical results corresponding to different degrees of rational approximation are shown in Fig. 5. Although there is no analytical solution available, it can be seen, that the numerical solutions are approaching each other for increasing degree of approximation M. The curves for $M = 7$ and 8 cannot be distinguished in Fig. 5.

According to Section 3.2, Eq. (76), the coupled system consisting of Euler–Bernoulli beam with vanishing Winkler foundation, $\beta = 0$, and vertical spring k is described by the following fractional differential equation in the time-domain:

$$k w_0(t) + 2\sqrt{2} EIC^{3/4} [{}_{-\infty}D^{3/2} w_0(t)] = F_0(t), \quad C = \frac{\rho A}{EI}. \tag{83}$$

Eq. (83) has also been solved numerically for the unit-impulse load (82) using a specific time-stepping scheme developed for fractional differential equations [27,26]. The resulting vertical displacement $w(x=0,t)$ at the point of excitation of the Euler–Bernoulli beam is compared to that of the Timoshenko beam in Fig. 6. It can be seen that the Euler–Bernoulli model leads to bigger maximum and minimum displacements due to the unit-impulse load. Moreover, a phase shift is visible in Fig. 6. However, the numerically obtained displacement curves corresponding to the two different beam models are similar, despite the big differences with respect to the dynamic stiffness.

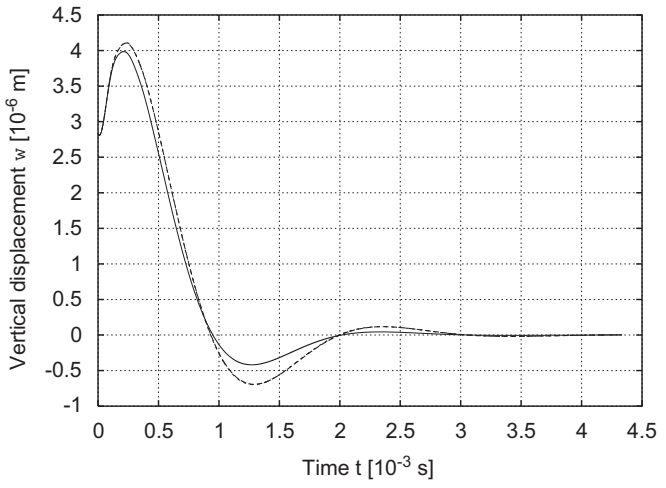

Fig. 5. Timoshenko beam supported by a single spring $k = 5.0 \times 10^8$ [N/m]. Vertical displacement $w(x=0,t)$ due to unit-impulse load (82). Time step: $h = 1.0 \times 10^{-7}$ s. ——— $M = 5$, — — — $M = 7$, - - - - - - $M = 8$.

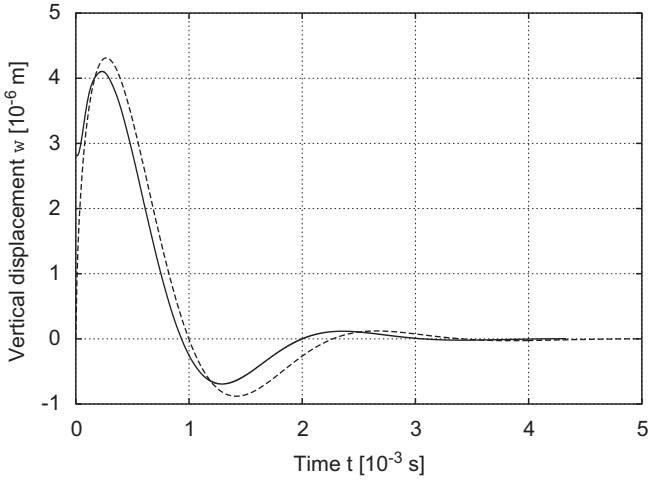

Fig. 6. Comparison of beam models in the time-domain. Vertical displacement $w(x=0,t)$ due to unit-impulse load (82). Time step: $h=1.0\times10^{-7}$ s. ——— Timoshenko, $M=7$, — — — — Euler–Bernoulli.

5. Conclusions

Based on a derivation of the translational and rotational dynamic stiffness of both infinite Timoshenko and Euler–Bernoulli beams on Winkler foundation in the frequency-domain, time-domain beam models have been obtained using the mixed-variables technique in this paper. Here, special emphasis has been placed on the high-frequency asymptotic behaviour of the respective dynamic stiffness formulations.

The use of Timoshenko's beam model leads to an asymptotic behaviour in the frequency-domain which is linear with respect to $i\omega$. Thus, the corresponding expression in the time-domain is a first-order time-derivative. The numerical solution in the time-domain can be obtained by classical time-solvers with local properties. Contrary to Timoshenko's model, Euler–Bernoulli's beam theory generates rational powers of $i\omega$ in the frequency-domain and consequently fractional derivatives in the time-domain with memory integrals to be solved. Their evaluation asks for nonlocal time-solvers with much higher computational effort than local solvers.

Considering the above computational benefits gained by including shear deformations in one-dimensional dynamic elasticity problems, parallels to static one- or two-dimensional problems can be drawn. It is well-known from mixed-methods in static finite element concepts [29] that shear deformations can be included not only for mechanical reasons, but also in order to optimize the discretization in the space-domain.

Summarizing, the main message of this paper is that the physically more realistic Timoshenko beam model offers additional numerical advantages when dealing with transient dynamic problems in unbounded domains.

References

[1] K. Popp, H. Kruse, I. Kaiser, Vehicle–track dynamics in the mid-frequency range, *Vehicle System Dynamics* 31 (1999) 423–464.
[2] L. Andersen, S.R.K. Nielsen, P.H. Kirkegaard, Finite element modelling of infinite Euler beams on Kelvin foundations exposed to moving loads in convected coordinates, *Journal of Sound and Vibration* 241 (4) (2001) 587–604.
[3] L. Sun, A closed-form solution of a Bernoulli–Euler beam on a viscoelastic foundation under harmonic line loads, *Journal of Sound and Vibration* 242 (4) (2001) 619–627.
[4] V.H. Nguyen, D. Duhamel, A new numerical approach for infinite Euler–Bernoulli beam on a Winkler foundation under high-velocity moving loads, in: H. Grundmann, G.I. Schuëller (Eds.), *Structural Dynamics, EURODYN 2002*, Swets & Zeitlinger, 2002.
[5] Y.H. Chen, C.Y. Li, Dynamic response of elevated high-speed railway, *Journal of Bridge Engineering, ASCE* 5 (2000) 124–130.
[6] Y.H. Chen, Y.H. Huang, C.T. Shih, Response of an infinite Timoshenko beam on a viscoelastic foundation to a harmonic moving load, *Journal of Sound and Vibration* 241 (2001) 809–824.

[7] M.H. Kargarnovin, D. Younesian, Dynamics of Timoshenko beams on Pasternak foundation under moving load, *Mechanics Research Communications* 31 (2004) 713–723.
[8] M.H. Kargarnovin, D. Younesian, D.J. Thompson, C.J.C. Jones, Response of beams on nonlinear viscoelastic foundations to harmonic moving loads, *Computers and Structures* 83 (2005) 1865–1877.
[9] J. Bitzenbauer, J. Dinkel, Dynamic interaction between a moving vehicle and an infinite structure excited by irregularities—Fourier transform solution, *Archive of Applied Mechanics* 72 (2002) 199–211.
[10] S. Timoshenko, D.Y. Young, *Vibration Problems in Engineering*, third ed., D. van Nostrand, New York, 1961.
[11] R.W. Traill-Nash, A.R. Collar, The effects of shear flexibility and rotatory inertia on the bending vibrations of beams, *Quarterly Journal of Mechanics and Applied Mathematics* VI (1953) 2.
[12] B. Dawson, Rotatory inertia and shear in beam vibration treated by the Ritz method, *Aeronautical Journal* 72 (1968) 341–344.
[13] N.G. Stephen, Considerations on second order beam theories, *International Journal of Solids and Structures* 117 (1981) 325–333.
[14] M.A. Moreles, S. Botello, R. Salinas, A root-finding technique to compute eigenfrequencies for elastic beams, *Journal of Sound and Vibration* 284 (2005) 1119–1129.
[15] Y.C. Fung, *Foundations of Solid Mechanics*, Prentice-Hall, Englewood Cliffs, 1986, pp. 322–325.
[16] H. Antes, M. Schanz, S. Alvermann, Dynamic analysis of plane frames by integral equations for bars and Timoshenko beams, *Journal of Sound and Vibration* 276 (2004) 807–836.
[17] L. Sun, An explicit representation of steady state response of a beam on an elastic foundation to moving harmonic line loads, *International Journal for Numerical and Analytical Methods in Geomechanics* 27 (2003) 69–84.
[18] P. Ruge, C. Trinks, Dynamics of infinite beams described by fractional time derivatives, *ASME* 19*th International Biennial Conference on Mechanical Vibration and Noise*, Chicago, IL, 2003; published on CD-ROM.
[19] P. Ruge, C. Trinks, Consistent modelling of infinite beams by fractional dynamics, *Nonlinear Dynamics* 38 (2004) 267–284.
[20] P. Ruge, C. Trinks, S. Witte, Time-domain analysis of unbounded media using mixed-variable formulations, *Earthquake Engineering and Structural Dynamics* 30 (2001) 899–925.
[21] G.R. Cowper, The shear coefficient in Timoshenko's beam theory, *ASME Journal of Applied Mechanics* 33 (1966) 335–340.
[22] R.D. Mindlin, H. Deresiewicz, Timoshenko's shear coefficient for flexural vibrations of beams, Report No. 10, ONR Project NR064-388, Department of Civil Engineering, Columbia University, New York, 1953.
[23] A.H.-D. Cheng, H. Antes, On free space Green's function for high order Helmholtz equations, in: S. Kobayashi, N. Nishimura (Eds.), *Boundary Element Methods, Proceedings of the IABEM91, Kyoto, Japan*, Springer, Berlin, 1992, pp. 67–71.
[24] L. Hörmander, *Linear Partial Differential Operators*, Springer, Berlin, 1963.
[25] I. Podlubny, Fractional differential equations, *Mathematics in Science and Engineering*, Vol. 198, Academic Press, New York, 1999.
[26] C. Trinks, Consistent Absorbing Boundaries for Time-domain Interaction Analyses Using the Fractional Calculus, Ph.D. Thesis, Technische Universität Dresden, Fakultät Bauingenieurwesen, 2004, available from: Carolin.Birk@tu-dresden.de.
[27] C. Trinks, P. Ruge, Description of wave propagation by fading memory, in: H. Grundmann, G.I. Schuëller (Eds.), *Structural Dynamics—EURODYN* 2002, *Proceedings of the 5th International Conference on Structural Dynamics*, Munich, Germany, 2–5 September 2002.
[28] C. Song, M.H. Bazyar, A boundary condition in Padé series for frequency domain solution of wave propagation in unbounded domains, *International Journal for Numerical Methods in Engineering* 69 (2007) 2330–2358.
[29] O.C. Zienkiewicz, R.L. Taylor, *The Finite Element Method*, fourth ed., Vol. 1, McGraw-Hill, New York, 1994.